Nanojacketing and Dejacketing of ds-DNA : A Non-destructive Characterization of Nanojacketed Sample by Impedance Spectroscopy.

ARTICLE *in* THE JOURNAL OF PHYSICAL CHEMISTRY B · FEBRUARY 2014

Impact Factor: 3.3 · DOI: 10.1021/jp412373m · Source: PubMed

4 AUTHORS, INCLUDING:

Sudipta Nandi

Indian Association for the Cultivation of Scie…

5 PUBLICATIONS **27** CITATIONS

SEE PROFILE

Aniruddha Kundu

Indian Association for the Cultivation of Scie…

8 PUBLICATIONS **94** CITATIONS

SEE PROFILE

THE JOURNAL OF PHYSICAL CHEMISTRY B

Article

pubs.acs.org/JPCB

Nanojacketing and Dejacketing of ds-DNA: A Nondestructive Characterization of a Nanojacketed Sample by Impedance Spectroscopy

Sudipta Nandi, Pratap Mukherjee, Aniruddha Kundu, and Arun K. Nandi*

Indian Association for the Cultivation of Science, Jadavpur, Kolkata 700 032, India

ABSTRACT: A facile approach of nanojacketing DNA in intact conformation is evolved by the in situ polymerization of *o*-methoxyaniline (OMA) at 30 °C using $HAuCl_4$ as an oxidant and DNA as a soft template. It concomitantly produces poly(*o*-methoxyaniline) (POMA) and a Au nanojacket encapsulating the double stranded DNA (ds-DNA). The POMA chains remain adhered to the Au nanojacket, facilitating the dissolution of nanojacketed DNA (DNA−Au−POMA) in organic solvent without affecting its conformation. Digestion of the nanojacketed system with saturated iodine solution dejackets the ds-DNA with retention of its conformation, leaving the POMA nanotube. The nanojacketing and dejacketing phenomena are established by transmission electron microscopy (TEM), UV−vis spectroscopy, and CD spectroscopy, and the nanostructure is further characterized by FTIR, X-ray diffraction (XRD), and X-ray photoelectron spectroscopy (XPS). The impedance study of the DNA−Au−POMA sample suggests the Cole−Cole plots at both the impedance and modulus planes and the values of capacitance and electron-transfer resistance of the material (R_{et}) are calculated to be 13.74 pF and 388 kΩ, respectively. The presence of a single Debye peak in both the impedance and modulus vs frequency plots suggests an isotropic nature of the system, and the frequency dependent ac-conductivity suggests the presence of short-range translational and reorientational (localized) hopping of charge carriers at lower and higher frequency region.

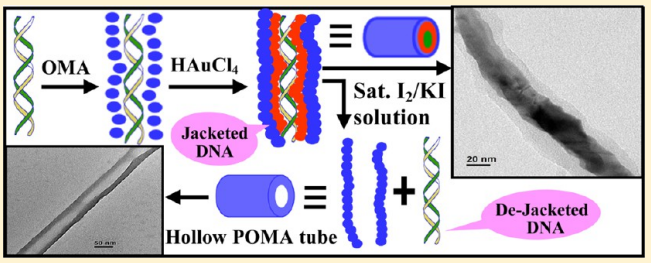

INTRODUCTION

Deoxyribonucleic acid (DNA), a long polymer chain of nucleotide units, is the most essential biomolecule for living organisms, which makes up the genetic component of all eukaryotes, bacteria, and many viruses. Most DNA possesses a double helical structure with negatively charged sugar−phosphate backbones and embedded nitrogenous base pairs where genetic information is stored in the sequence of these bases. This unique double helical structure of DNA with the stack of π electrons in the base pair not only makes it the genetic carrier but also promotes the possibility of DNA to form a "molecular conduit",[1] which makes it one of the promising molecules for nanotechnological applications. It also has the ability to accumulate metal ions which may be reduced to metal nanoparticles, nanorods, and nanowires following the contour of a DNA template.[2−7] Therefore, the association of DNA and nanomaterials could bring about very intriguing physicochemical properties useful for advanced molecular electronics,[8−11] fluorescent biological labeling for medical diagnostics,[12,13] and biofunctionalized ordered structural growth.[14] On the other hand, DNA can act as a good template for the directed growth of conducting polymers[15−19] and the so formed DNA-conducting polymer hybrid finds wide application in the study of DNA hybridization,[20,21] gene therapy,[22,23] genoelectronics,[22,23] and various biosensing applications.[1,23−25] Although DNA is easy to modify for such novel, tailor-made applications, it also has a major limitation because of its poor solubility in organic solvent, where it loses its base pairing recognition properties. Making DNA soluble in organic solvents with retention of its biologically important properties becomes an attractive research area. For this purpose, cationic amphiphiles such as surfactants, lipid molecules, and cationic copolymers have been used to make DNA soluble in organic solvents, mainly chloroform.[26−28]

Among the various conducting polymers, polyaniline (PANI) has widely been studied due to the ease of its preparation and its ability to respond to various external stimuli by a change in electrical, optical, or chemical properties.[29] Polymerization of a substituted aniline derivative has also attracted a great deal of attention in the scientific community, since they exhibit similar opto-electrical properties like PANI. Recently, researchers have been interested in synthesizing poly(o-methoxyaniline) (POMA), a homopolymer of substituted aniline, due to its improved solubility in organic solvents compared to PANI.[30] For this purpose, various groups have adopted different techniques to synthesize POMA like electrochemical polymerization,[31] chemical oxidative polymerization,[32,33] and less common methods such as solid-state polymerization[34] and high-temperature polymerization.[35] Previously from our laboratory, Dawn et al. reported the interaction between

Received: December 18, 2013
Revised: January 21, 2014

dx.doi.org/10.1021/jp412373m | *J. Phys. Chem. B* XXXX, XXX, XXX−XXX

DNA and POMA, where DNA immobilizes ~30 POMA chains for a constant doping level of POMA.[36] This phenomenon motivates us to synthesize POMA using DNA as a soft template which can lead to wrapping DNA during the in situ synthesis of POMA.

Here we have used $HAuCl_4$ as an oxidant instead of ammonium persulphate (APS), since Huang et al. have reported that $HAuCl_4$ has the ability to polymerize aniline.[37] Though *o*-methoxyaniline (OMA) is just a substituted aniline, this substitution often causes difficulty for its polymerization, and to the best of our knowledge, there is no report on synthesizing poly(*o*-methoxyaniline) (POMA) using $HAuCl_4$ as an oxidant. In our work, $HAuCl_4$ has simultaneously polymerized *o*-methoxyaniline and itself become reduced to the Au nanoparticles (AuNPs) which are accumulated on the DNA surface in a closely spaced fashion, producing *nanojacketed* DNA where POMA chains remain adhered to the *nanojacket* stabilizing the dispersion. This simple approach promotes the transfer of DNA from aqueous to organic medium sustaining the helical conformation of DNA within the nanojacket. Also, it would be interesting if we could dejacket DNA without changing its conformation and make it soluble again in water. Thus, we have developed a simple process to dejacket DNA from the nanojacketed structure using saturated I_2 solution, retaining the double helical conformation of DNA and leaving the hollow POMA nanotube. The nanojacketing and dejacketing phenomena have been characterized with the help of transmission electron microscopy (TEM) and Fourier transformed infrared (FTIR), UV−vis, circular dichroism (CD), and X-ray photoelectron (XPS) spectroscopic techniques.

Impedance spectroscopy is a nondestructive characterization technique that provides electrical information in the frequency domain,[38,39] and it has been extensively used to investigate the dynamics of bound or mobile charge in the bulk or interfacial regions of any kind of solid or liquid material of ionic, semiconducting, mixed electronic−ionic, and even insulating character.[40−44] As the DNA molecule consists of a double helical structure due to the π stacking of the conjugated base pair, that can also constitute the pathway for electron transport; thus, impedance data may give useful insight into the electrical behavior of the nanojacketed system. Here we have studied the impedometric behavior of the as prepared DNA−Au−POMA *nanojacketed* material to get an idea about the dynamics of bound or mobile charge. The ac-conductivity measurement from the impedance data is also used to understand the conduction mechanism of the system.

EXPERIMENTAL SECTION

Materials. Calf thymus DNA (type 1; sodium salt) and chloroauric acid ($HAuCl_4$) were purchased from Sigma-Aldrich Co., USA. Hydrochloric acid (HCl), *o*-methoxyaniline (OMA), iodine (I_2), and potassium iodide (KI) were purchased from E-Merck (Mumbai). OMA was distilled, and the middle fraction of the distillate was used. Other reagents were used as received. All the experiments were done in sterilized triple distilled water, and the experiments involving DNA were performed under sterilized conditions. To replace the sodium ion of DNA by a proton, its aqueous solution (20 mg of NaDNA in 2 mL of water) was mixed with 0.01 N HCl solution (3 mL) and the mixture was dialyzed in sterilized dialysis paper to remove sodium, chloride, and excess hydrogen ions. The above ions were frequently monitored using silver nitrate solution, and the dialysis was continued until all the chloride ions were removed. After the dialysis process, the solution is used as a protonated DNA solution.

Synthesis. *One-Pot Synthesis of Au Nanoparticles and Poly(O-methoxyaniline) Coated DNA, i.e., Nanojacketed DNA.* At first, 15 μL of distilled *o*-methoxyaniline was added to the above protonated DNA solution and was stirred for 1 h to dissolve in the aqueous medium. An aqueous solution of chloroauric acid (15.7 mg/mL) was then added dropwise to the above mixture with stirring conditions. The polymerization of *o*-methoxyaniline monomer was visualized from the generation of blue-violet color of the solution, which becomes more and more intense with progress of reaction time. After allowing the solution at the same stirring conditions to react overnight at room temperature, a dark violet color of the solution was observed. The resultant material was isolated by centrifuging in a Beckman Coulter centrifuge (Allegra 64R model), was washed repeatedly with triple distilled water, and was then freeze-dried. Finally, an aqueous solution and also a chloroform solution of this material were prepared by rigorous stirring and were used as the solution of the novel nano-biocomposite for all the characterization studies. A similar experiment was done for the polymerization of POMA following the same procedure except addition of DNA.

Dejacketing of DNA from the DNA−Au−POMA Nano-Biocomposite. A portion of the above nano-biocomposite was treated with saturated iodine solution and was kept for 5 h. Then, the resulting solution was dialyzed against triple distilled water until the solution became free from iodine, iodide, and Au^{3+} ions. The dialyzed solution was centrifuged, and both the residue and the supernatant part were collected. The residue was dissolved into chloroform for spectroscopic studies.

Characterization. *Microscopy.* The shape, size, and dispersity of the Au nanoparticles were monitored by transmission electron microscopy (TEM JEOL, 2010EX) operated at an acceleration voltage of 200 kV and fitted with a CCD camera. A specimen for TEM study was made by spreading a small drop of $CHCl_3$ solution of prepared materials on a carbon-coated copper grid and allowing the drop to dry completely in air and finally in a vacuum at 30 °C. The electron diffraction experiment was carried out on a Au nanoparticle observed in the TEM micrograph, and the crystal spacing (d_{hkl}) values were calculated directly by measuring the distance between the opposite spots on the same circumference of the diffraction pattern using the Image J software. Energy-dispersive X-ray (EDX) analysis was done to determine the elemental composition of the composite.

Spectroscopy. The UV−vis absorption spectra of the solutions were taken from a UV−Vis spectrophotometer (Hewlett−Packard, model 8453) in a quartz cell of 1 mm thickness in the wavelength range 190−1100 nm at 30 °C. The circular dichroism (CD) spectra of the solutions were made using a spectro-polarimeter (JASCO, model J-815) in a 1 cm quartz cuvette at 30 °C. The FT-IR spectra of the samples were taken in a Perkin-Elmer FT-IR instrument (spectrum100) using KBr pellets of the solid samples (freeze-dried). The XRD study was performed using a Seifert X-ray diffractometer (model C-3000) in reflection mode with a parallel beam optics attachment. Nickel-filtered copper Kα radiation (λ = 0.154 nm) operating at a 35 kV voltage and a 30 mA current was used. The samples were scanned from 2θ = 5° to 2θ = 90° at the step scan mode (step size 0.03°, preset time 2 s), and the diffraction pattern was recorded using a scintillation counter

dx.doi.org/10.1021/jp412373m | J. Phys. Chem. B XXXX, XXX, XXX−XXX

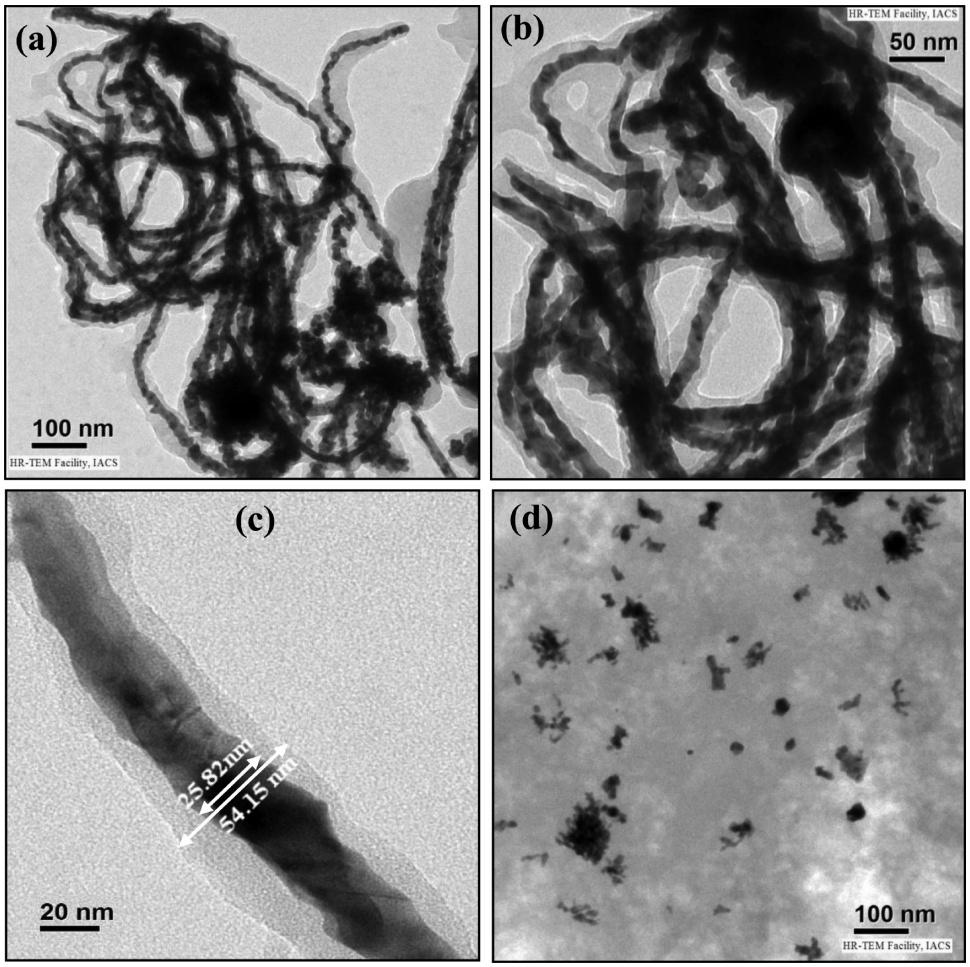

Figure 1. TEM images of Au–POMA material obtained (a, b, and c) in the presence of DNA at different magnifications and (d) in the absence of DNA.

detector. The X-ray photoelectron spectroscopy (XPS) of DNA–Au–POMA material was performed using a focused monochromatized Mg Kα X-ray source (1253.6 eV) in the XPS instrument (Omicron NanoTechnology 057).

The impedance spectroscopic measurements were done by sandwiching the sample between two ITO conducting strips of 2 mm width placed perpendicularly with each other, and it was connected through the connecting wires of the impedance meter using Ag paste. The measurements were performed at 30 °C temperature over the frequency range $1-10^6$ Hz for an oscillation voltage of 100 mV at 0 V DC level using a Solartron SI 1260 Impedance analyzer (Solartron, U.K.).

RESULTS

Morphology. The structure and orientation of the Au nanoparticles produced concurrently with the formation of POMA can be observed from the transmission electron microscopy (TEM) images (Figure 1), which clearly indicate that the AuNPs (darker contrast) are generated homogeneously with concomitant formation of POMA (brighter contrast) in both the presence and the absence of DNA. In the presence of DNA, the so formed AuNPs are accumulated on the DNA surface and long cylinder-like nanostructures (*nanojacket*) are produced due to the agglomeration of closely spaced AuNPs, as shown in Scheme 1. The brighter layer at the surroundings of AuNPs indicates the simultaneous formation of POMA, which builds an outer coating upon the Au *nanojacket* structure. The average outer diameter of this overall cylindrical structure is 54.15 ± 2.31 nm with a core diameter of 25.82 ± 1.66 nm comprised of the jacketed DNA by AuNPs (Figure 1c). In the micrographs, DNA fibers inside the nanojacket are not separately observed probably because of the darker contrast of the Au nanojacket. Therefore, from the TEM images, we can argue that the DNA becomes wrapped by AuNPs in the form of a nanojacket and the POMA layers adhered on its surface stabilize the nanojackets from collapsing with others by imparting steric hindrance. The POMA chains present at the shell assist the DNA to solubilize in organic medium along with the retention of its own conformation to be discussed later. Here it is necessary to get a quantitative idea on the nanojacket morphology particularly on the thickness of the core and the shell. From our previous study on the morphology of dsDNA, we have observed that our dsDNA has fibrillar morphology with a fibrillar diameter of 10.4 nm.[36] Assuming the nanojacket to be formed coaxially with the DNA fibril, the core and total diameter values are used to calculate the thickness of the Au nanojacket. The average thickness of the Au core in the nanojacket is found to be 7.71 nm, and that of the POMA shell is calculated to be 14.17 nm. These results suggest a true nanojacketing of dsDNA following the above simple redox polymerization technique of POMA by $HAuCl_4$.

dx.doi.org/10.1021/jp412373m | J. Phys. Chem. B XXXX, XXX, XXX–XXX

Scheme 1. Schematic Illustration of the Formation of Nanojacketing and Dejacketing Phenomena of ds-DNA with AuNPs and Simultaneous Formation of a POMA Nanotube

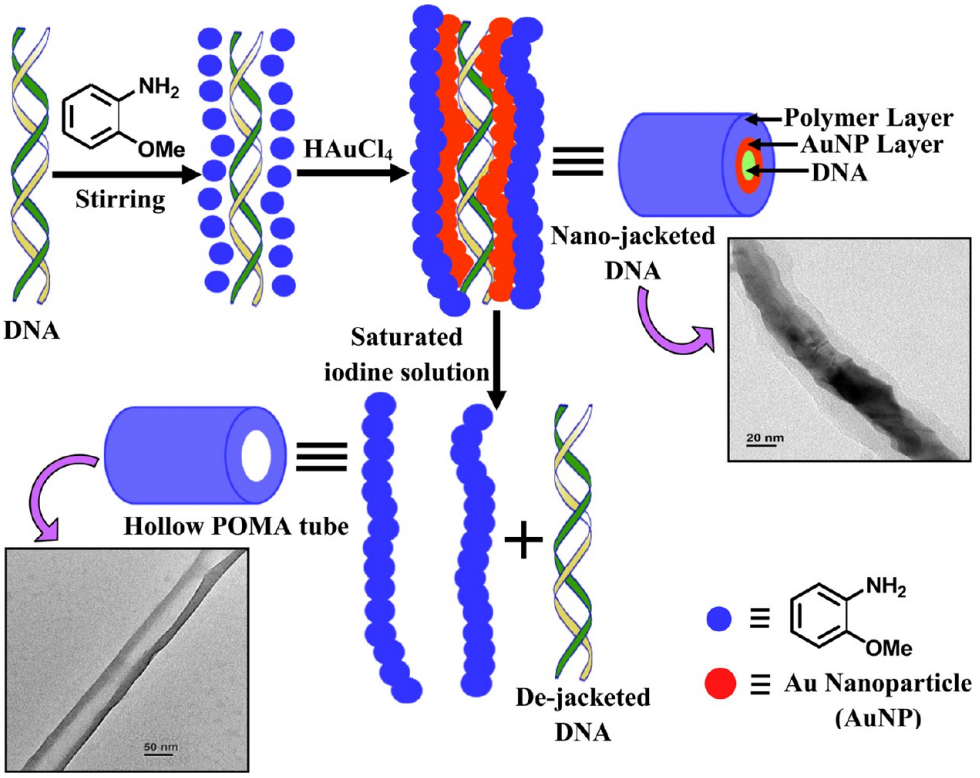

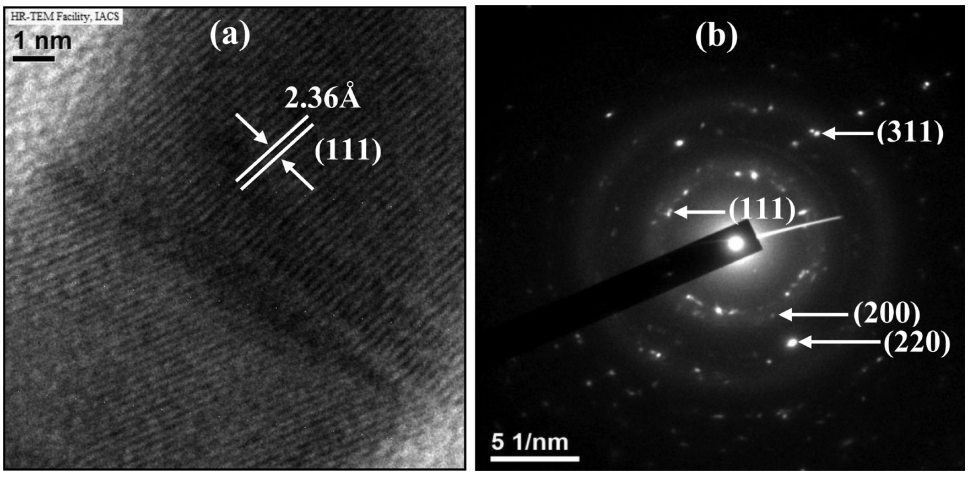

Figure 2. (a) HRTEM image and (b) electron diffraction pattern of AuNPs present in synthesized DNA−Au−POMA nanojacketed material.

From the HRTEM image (Figure 2a), the distinct fringe pattern of Au nanojackets is observed, providing clear evidence of the crystalline nature of AuNPs. The interplanar distance of 2.36 Å obtained from the fringe pattern represents the (111) lattice planes of Au nanocrystals. The electron diffraction pattern (Figure 2b) of the prepared DNA−Au−POMA nanobiocomposite confirms the presence of (111), (200), (220), and (311) Miller planes of the Au nanocrystals. The presence of all the components (POMA, Au, and DNA) is evidenced from the presence of N, P, Au, etc., in the EDX spectrum (Figure 3).

In the absence of DNA, the *nanojacket* morphology is not produced (Figure 1d), which indicates that due to the lack of DNA template so formed AuNPs cannot accumulate in a regular fashion required for the formation of *nanojacket* morphology. However, in this case also, the crystalline nature of AuNPs is retained (Figure 4a) and the presence of (111), (200), (220), and (311) Miller planes of Au nanocrystals is also evident from the electron diffraction pattern (Figure 4b).

Being curious whether the nanojacketed morphology can be dejacketed keeping the DNA structure intact, we have treated the DNA−Au−POMA composite with saturated aqueous iodine solution in KI[37] and the AuNPs of the nanojacket become oxidized to Au^{3+} ions dejacketing the DNA. This leaves the hollow POMA nanotube (Figure 5), and DNA becomes free to move into the aqueous medium. From Figure 5, we have measured the diameter of the POMA nanotube as 54.59 ± 1.67 nm with an inner diameter value of 25.92 ± 1.08 nm, which are

dx.doi.org/10.1021/jp412373m | J. Phys. Chem. B XXXX, XXX, XXX−XXX

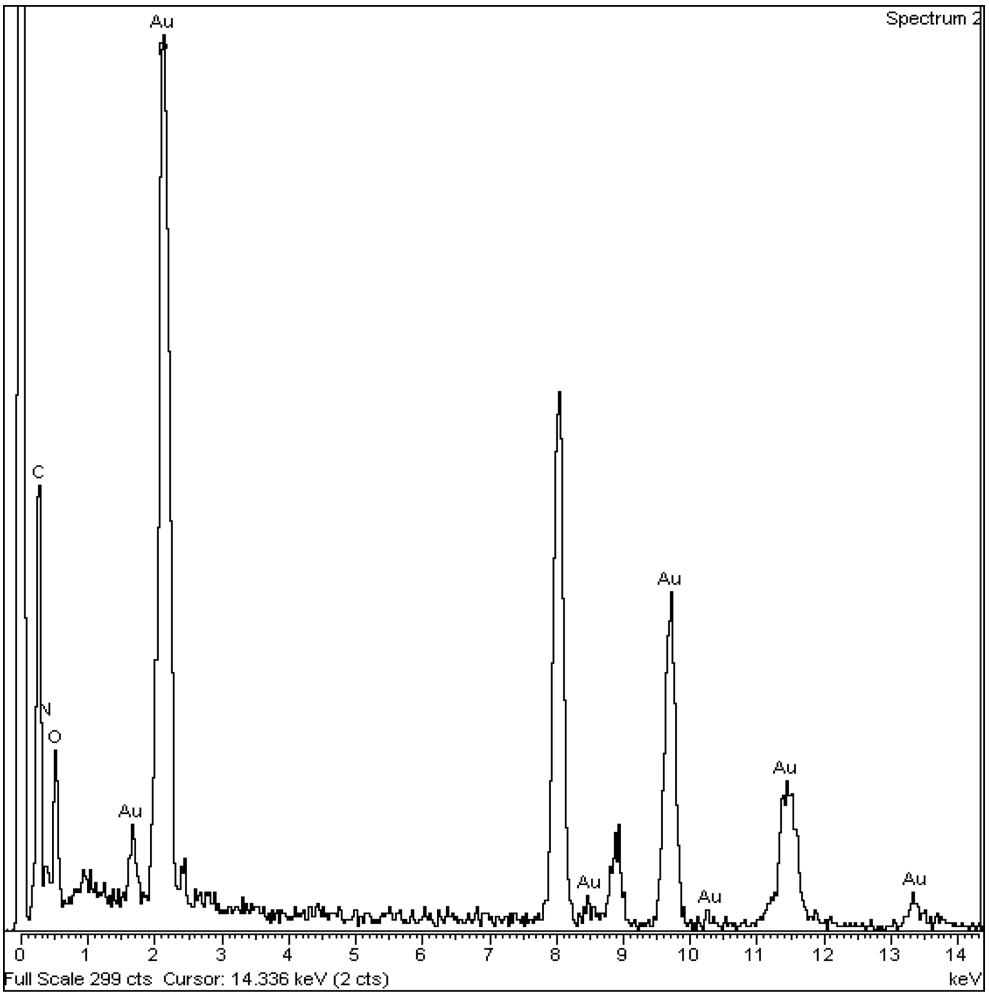

Figure 3. The EDX spectrum of the composite confirming the presence of DNA, POMA, and AuNPs in the nanojacket. The peaks at 8 and 9 keV are of Cu.

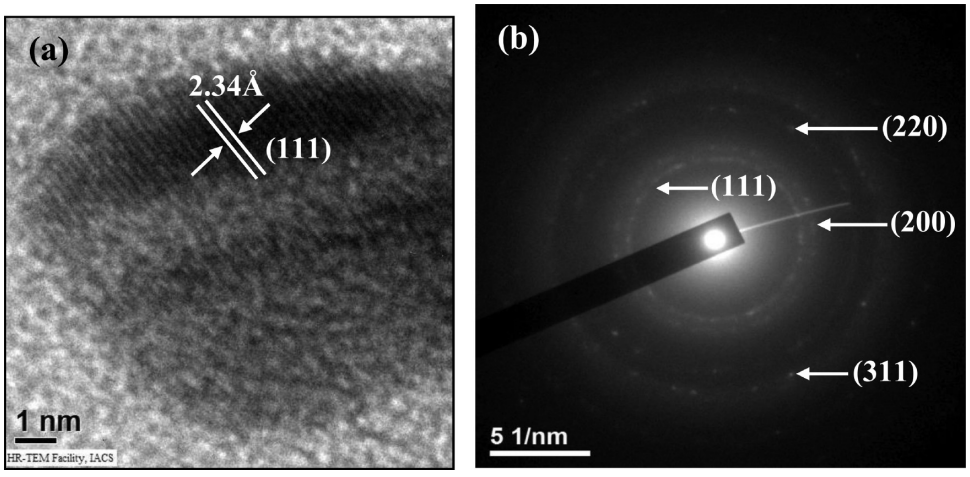

Figure 4. (a) HRTEM image and (b) electron diffraction pattern of AuNPs present in the Au–POMA materials prepared without DNA.

very similar to the average diameter of POMA in the so formed DNA–Au–POMA hybrid, i.e., nanojacketed DNA. The dejacketing phenomenon is also illustrated in Scheme 1.

Spectral Characterization. *UV–vis Spectroscopy.* From the UV–vis spectra (Figure 6), the presence of AuNPs and concomitant formation of POMA is ascertained. For the nanojacketed DNA, the absorption peak of DNA base pairs at 270 nm suggests the presence of DNA, while those at 284, 314, 422, and 542 nm designate the formation of POMA (Figure 6a). Usually the $\pi-\pi^*$ transition peak of DNA base pairs arises at 262 nm,[45,46] and here a red shift of 8 nm occurs. One possible reason may be due to the lowering of the band gap for easier π-stacking of the DNA bases in the nanojacketed state where the cohesive force between the walls of the nanojacket

dx.doi.org/10.1021/jp412373m | J. Phys. Chem. B XXXX, XXX, XXX–XXX

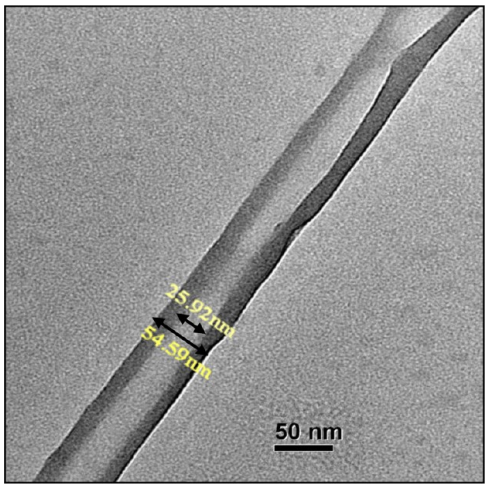

Figure 5. TEM images of the as prepared nano-biocomposite after treatment with saturated iodine solution.

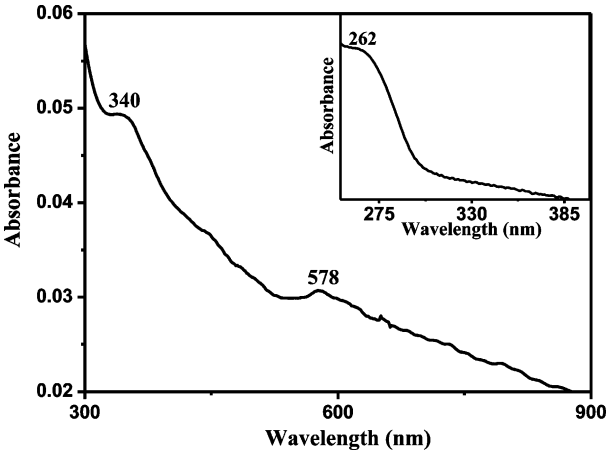

Figure 7. UV–vis spectra of $CHCl_3$ solution. Inset: aqueous solution of DNA–Au–POMA material after dejacketing.

may facilitate better stacking of the π orbitals. The peak at 284 nm may arise from the aromatic ring absorption,[47] and that at 314 nm (hump) originates from the $\pi-\pi^*$ transition of the benzenoid ring of POMA. The peak at 422 nm indicates a polaron band to π^* band transition of POMA which is in the doped state.[48] The peak at 542 nm is generated due to the combined plasmon band of AuNPs[49] and n–π^* transition of doped POMA.[50] In the absence of DNA, concomitant polymerization of OMA and formation of AuNPs also occur, as evident from the appearance of peaks at 283, 311, 421, and 535 nm (Figure 6b). Here both peaks at 311 and 421 nm are observed, which indicate that in this case also doped POMA is formed. The peak at 535 nm confirms the presence of AuNPs. After dejacketing of DNA–Au–POMA nanocomposite by treatment with iodine solution, the aqueous supernatant part shows a peak at 262 nm (Figure 7, inset) which corresponds to free ds-DNA and the chloroform solution of the precipitate exhibits peaks at 340 and 578 nm (Figure 7) which are assigned to the $\pi-\pi^*$ transition and n–π^* transition of undoped POMA, respectively.[51] Thus, the UV–vis spectra clearly indicate the presence of DNA within the nanojacket and it is completely recoverable in the intact form in the dejackated state.

CD Spectroscopy. The CD spectrum of nanojacketed DNA in organic solvent ($CHCl_3$) and that of dejacketed DNA in aqueous solution are presented in Figure 8. In $CHCl_3$ solution, the nanojacketed DNA exhibits a positive peak above 240 nm and a negative peak below 240 nm (Figure 8a), which signifies that the secondary structure of DNA remains intact.[28] Dejacketed DNA in aqueous solution demonstrates two positive peaks at 277 and 216 nm and one negative peak at 243 nm (Figure 8b) which are typical for the B conformation of DNA.[45,51,52] This leads us to conclude that in our procedure DNA acts as a soft template for linear growth of Au nanocrystal to produce the Au nanojacket upon which polymerization of OMA takes place simultaneously and makes a coat over the outer surface of AuNPs, thereby protecting it from coalescence with other nanojackets. After oxidization of AuNPs by saturated iodine solution, DNA becomes free and moves to an aqueous medium with a complete retention of its secondary structure.

FTIR Spectroscopy. The molecular structure of the as prepared nano-biocomposite was further characterized by FTIR spectroscopy (Figure 9). At first, the formation of POMA can be manifested from the appearance of the peaks at 1580 cm^{-1} (quinoid ring deformation), 1514 cm^{-1} (deformation of the benzenoid ring), 1250 cm^{-1} (C—N stretching vibration), 1210 cm^{-1} (secondary aromatic amine stretching), and 1117 cm^{-1}

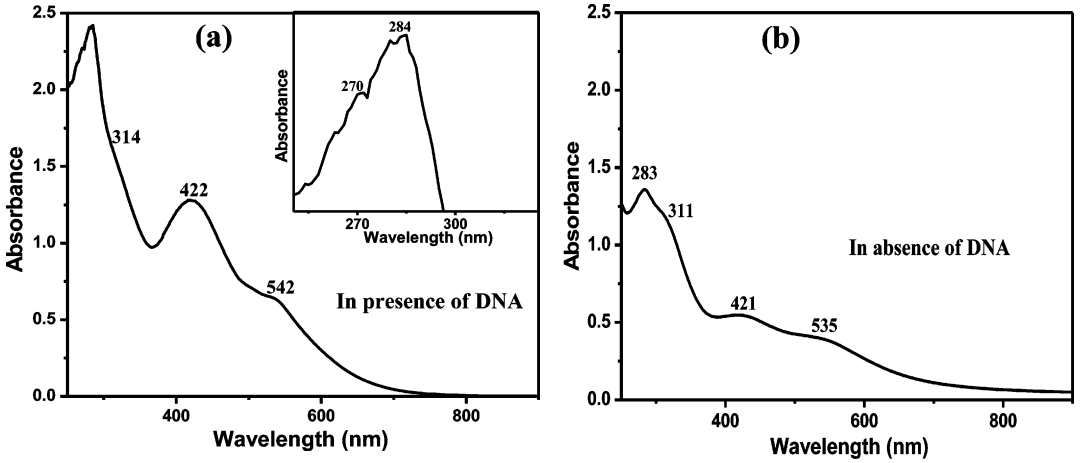

Figure 6. UV–vis spectra of the $CHCl_3$ solution of synthesized nanomaterials (a) with DNA and (b) without DNA. Inset of part a: an enlarged part of the spectrum in part a.

dx.doi.org/10.1021/jp412373m | J. Phys. Chem. B XXXX, XXX, XXX–XXX

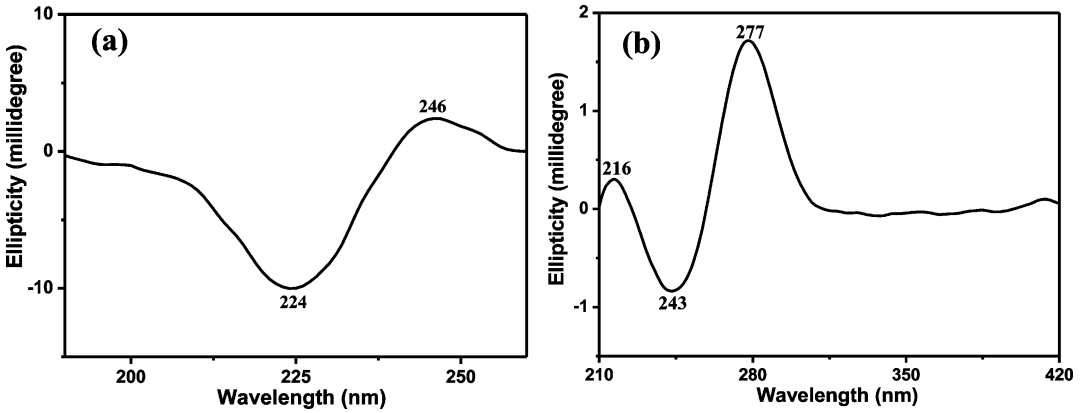

Figure 8. CD spectra of DNA in (a) $CHCl_3$ solution in jacketed state and (b) aqueous solution in dejacketed state.

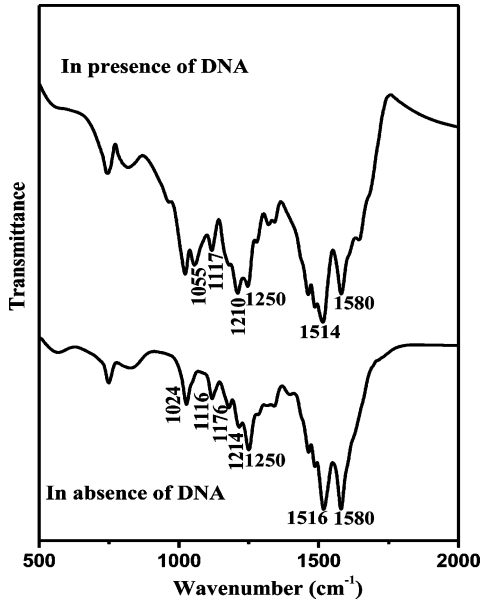

Figure 9. FTIR spectra of POMA–Au materials obtained in the presence of DNA and in the absence of DNA.

for the C—H in-plane bending vibration. The frequency of the benzenoid ring deformation is blue-shifted to 1514 cm^{-1} from the reported value (1483 cm^{-1}),[53] indicating the interaction between the nitrogen atom of the so formed POMA and AuNPs. Further, POMA has a vibration peak at 1161 cm^{-1} arising from the quinoid (N═Q═N) vibration associated with the partial electron-like structure[51−54] which is shifted to 1185 cm^{-1} because AuNPs are stabilized through nitrogen atoms of POMA, causing doping of POMA.[53] On the contrary, the 1701 cm^{-1} peak of pure DNA, attributed to the in-plane deformation of the O—H groups of phosphoric acid,[36] is absent in the DNA–Au–POMA composite, indicating that the phosphoric acid group of DNA may also be engaged in the complex formation with the Au doped POMA. Due to the same reason, the 1067 cm^{-1} peak of pure DNA, depicted for the asymmetric stretching of a P–O–C vibration,[36] is also shifted to lower frequency at 1055 cm^{-1} in the DNA–Au–POMA composite. In the absence of DNA, all the characteristic peaks of POMA are present but the quinonoid (N═Q═N) vibration peak at 1161 cm^{-1} is shifted to 1176 cm^{-1}, which represents stabilization of AuNPs by POMA.[53] It is to be noted that the shift is ∼9 cm^{-1} lower here than that of the nanojacketed state probably because of the presence of more closely spaced AuNPs in the jacket causing stronger binding.

X-ray Diffraction (XRD) Study. The XRD patterns (Figure 10) clearly indicate the diffraction peaks of Au nanocrystals in

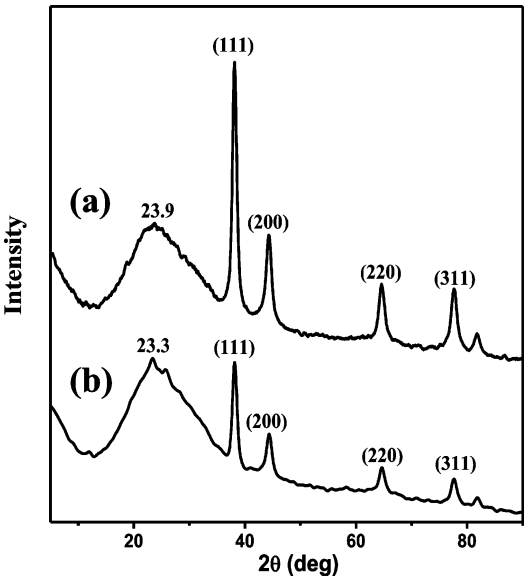

Figure 10. XRD patterns of POMA–Au materials produced (a) in the presence of DNA and (b) in the absence of DNA.

both DNA–Au–POMA nanojacket and Au–POMA nanocomposite systems, and the peak positions match very well with each other. However, the slightly different peak position of POMA in the presence of DNA (2θ = 23.9°) than that in the absence of DNA (2θ = 23.3°) is probably due to different POMA morphology as well as different extent of doping of POMA.[55]

XPS Study. The survey scan XPS spectrum of DNA–Au–POMA composite is shown in Figure 11a, which exhibits the presence of C, O, N, P, and Au^0 supporting the presence of POMA, DNA, and Au nanocrystals. The presence of DNA in DNA–Au–POMA composite is further confirmed from the enlarged XPS spectrum shown in Figure 11b, which reveals that the peak at 130 eV is originated from the core P_{2p} electron corresponding to the phosphoester bonding of DNA. The small shift in binding energy from 132.2 to 130 eV suggests the interaction between AuNPs and the phosphate group of DNA[56] in the DNA–Au–POMA composite, which indicates the

dx.doi.org/10.1021/jp412373m | J. Phys. Chem. B XXXX, XXX, XXX–XXX

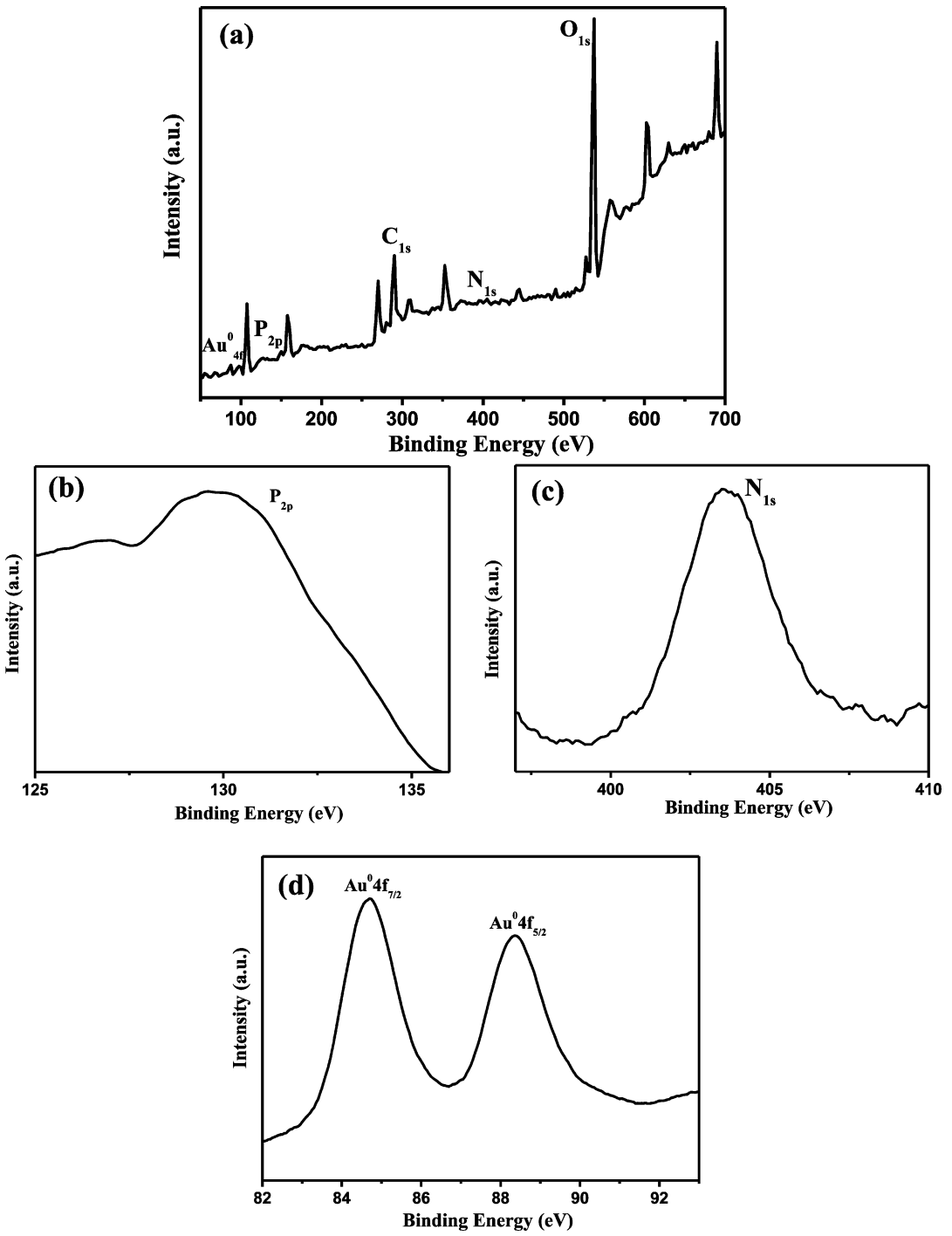

Figure 11. XPS spectra of DNA–Au–POMA nanojacketed material: (a) full scan; (b) P_{2p} peak; (c) N_{1s} peak; (d) Au^0 4f peaks.

formation of a Au nanojacket surrounding DNA. The N_{1s} core level peak of the sample at 403 eV (Figure 11c) may be assigned mainly to the nitrogen of the polymer in doped state.[57] The formation of gold nanoparticles during nanojacket formation has also been confirmed from XPS study shown in Figure 11d, which reveals a doublet peak of the Au^0 4f core level at 84.8 and 88.4 eV, respectively.[58,59]

Impedance Study. Impedance spectroscopy is an effective nondestructive technique to probe the inherent features of different materials.[60−63] For obtaining impedance, a small amplitude of AC voltage was applied across the sample. We examined that, for 100 mV, the sample response was good for obtaining data and a voltage lower than 100 mV was not usable for this sample. In our experiment, 100 mV was used as perturbed voltage applied on pure DC voltage (0 V). The impedance spectrum of the DNA–Au–POMA system is shown in Figure 12a and b as Nyquist plots [impedance imaginary part (Z'') vs its real part (Z') and electric modulus imaginary part (M'') vs its real part (M')] where both represent a typical Cole–Cole plot in the complex impedance and modulus planes at 30 °C. In order to interpret the above plots, it is essential to have an equivalent circuit model, which could provide insight into the electrical properties of the system. It is clear from Figure 12b that a single semicircle exists in the modulus plane,

dx.doi.org/10.1021/jp412373m | J. Phys. Chem. B XXXX, XXX, XXX–XXX

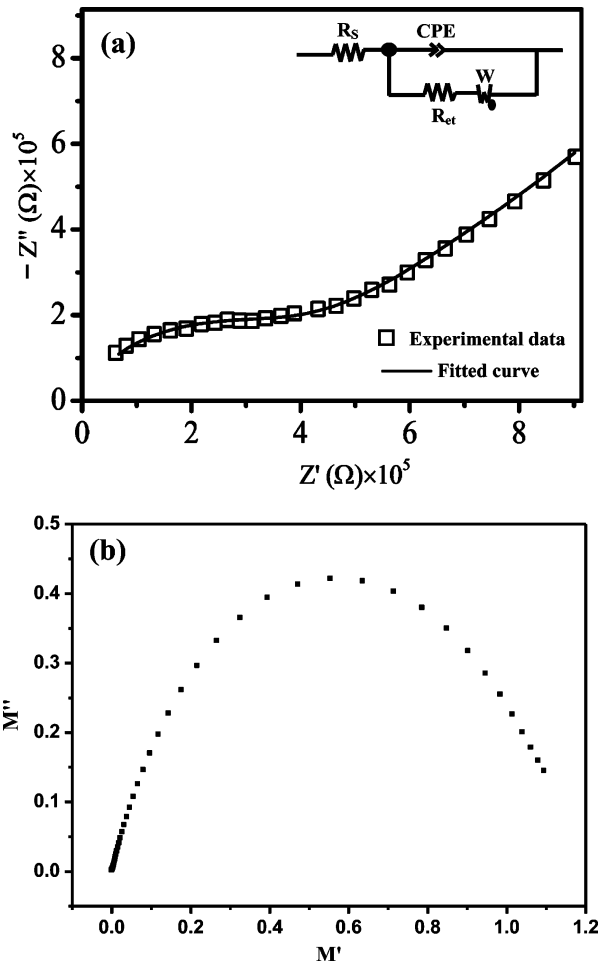

Figure 12. (a) Impedance Z'' (imaginary) spectroscopic plot against impedance real (Z'). Inset: equivalent circuit model. (b) Modulus M'' (imaginary) spectroscopic plot against modulus M' (real) for DNA–Au–POMA.

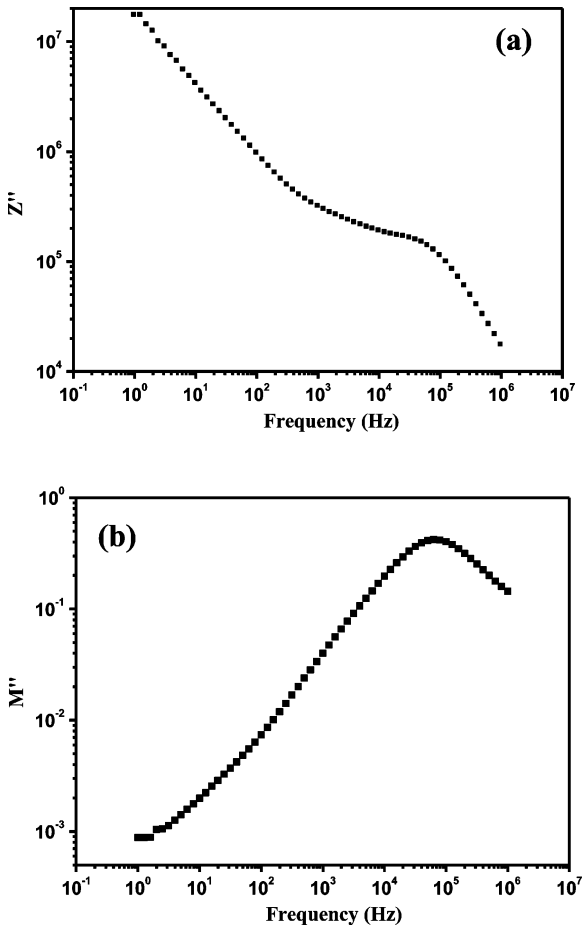

Figure 13. (a) Impedance Z'' (imaginary) spectroscopic plot against frequency. (b) Modulus M'' (imaginary) spectroscopic plot against frequency for DNA–Au–POMA.

but it fails to produce the semicircle in the complex impedance plane where the spectrum presumes a semicircle and a linear portion. The Nyquist plot signifies the existence of both resistive (R) and capacitive (C) features in the material,[31,60] and the impedance data (Figure 12a) has been fitted with commercial Z view software (version 3.2) shown by a solid line. In the inset of Figure 12a, we have drawn an equivalent circuit model that consists of the ohmic resistance of the electrode (R_S) in series with a constant phase element (CPE) and impedance in parallel.[62] The fitting of one measured spectrum to the equivalent circuit indicates the values of capacitance and electron-transfer resistance of the material (R_{et}) to be 13.74 pF and 388 kΩ, respectively. Thus, the DNA–Au–POMA nanojacket system exhibits both resistive and capacitive properties. This is possibly due to the π stacking of the conjugated base pairs of ds-DNA that constitute a separate transport pathway where charges may get accumulated, inducing the capacitive property.

The frequency dependence of the imaginary component (Z'') of impedance (Figure 13a) exhibits the presence of a single Debye peak. To confirm the presence of one Debye peak, we have also plotted an imaginary modulus component (M'') vs frequency (Figure 13b) which confirms the presence of a single Debye peak. Thus, the presence of a single Debye peak in both Z'' vs frequency and M'' vs frequency signifies the isotropic nature of the sample. The semicircle portion at higher frequencies (Figure 13a) corresponds to the electron-transfer-limited process, and the linear portion at lower frequencies represents the diffusion-limited process.[62]

The ac-conductivity of the sample is plotted with angular frequency and is shown in Figure 14. From the figure, it is evident that the conductivity at first increases linearly in the

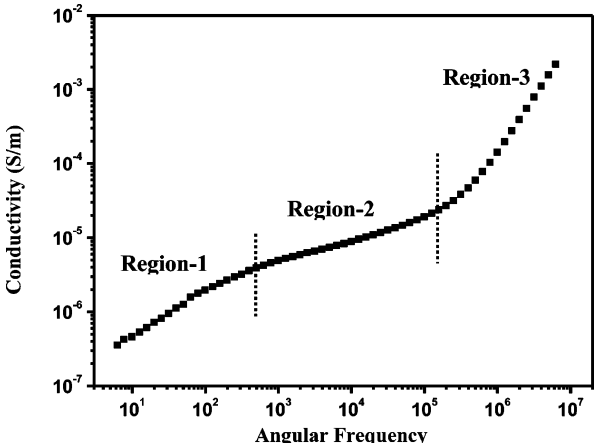

Figure 14. ac-Conductivity against angular frequency plot for DNA–Au–POMA material.

dx.doi.org/10.1021/jp412373m | J. Phys. Chem. B XXXX, XXX, XXX–XXX

Scheme 2. Schematic Representation for the Formation of an Intermediate $[DNA-AuCl_3]^-$ Complex to Produce a DNA–Au–POMA Nanojacket

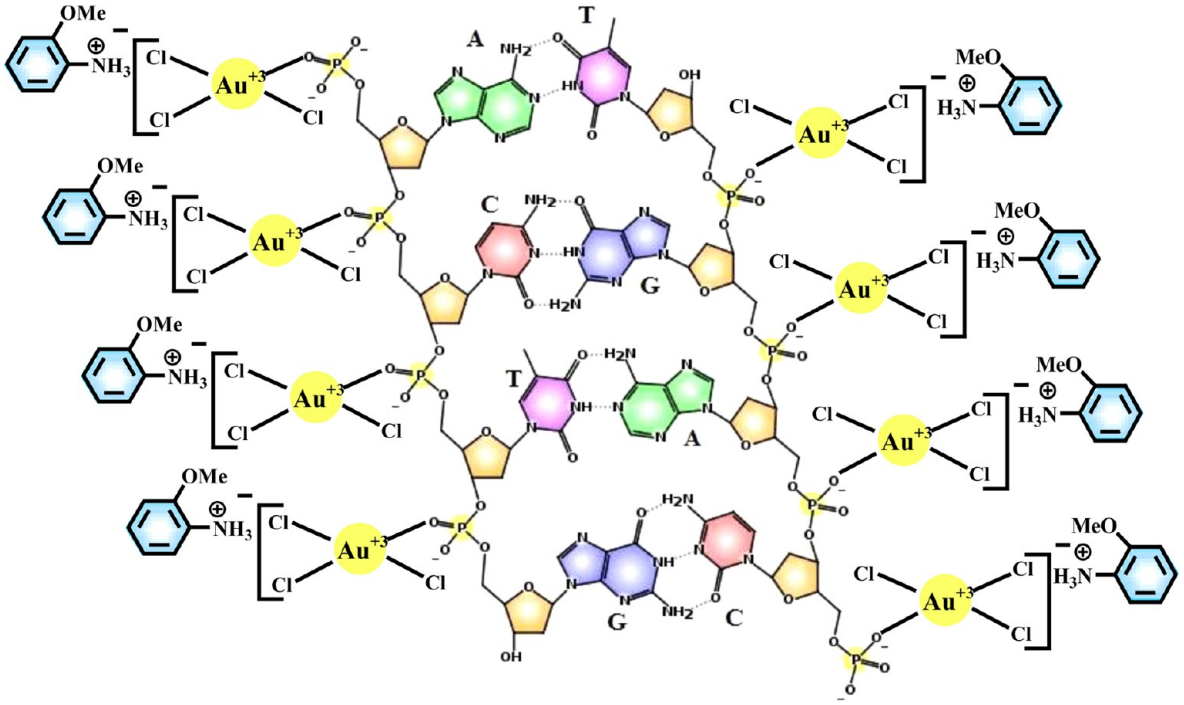

frequency ranges $1-5 \times 10^2$ Hz, then up to 10^4 Hz the rate of increase is lower, and beyond 10^5 Hz a sharp increase in conductivity with frequency is observed. Usually the frequency dependency of ac-conductivity is explained from the double power law:[64]

$$\sigma(\omega) = \sigma(0) + A_1\omega^{n1} + A_2\omega^{n2} \quad (1)$$

where $\sigma(0)$ is the frequency-independent conductivity, and it is absent here, though it was observed in the RNA–polyaniline–Au system.[60] A is a coefficient and n is an exponent which depend on the intrinsic property of the sample and temperature. The last term of the equation corresponds to the localized hopping that takes place for the very fast (i.e., low time period) motion. Here the long-range translational hopping is absent, showing the absence of frequency independent conductivity, but in the RNA–PANI–Au system, the long-range translational hopping exists probably due to the dendritic morphology of Au and the higher conductivity of RNA than that of DNA.[60] However, here in both regions 1 and 2 the short-range translational hopping comprised of two competing transport processes [(i) the jumping ion jump-back to its initial position, i.e., an unsuccessful hopping, and as a result (ii) the neighboring ions relax in a new site, i.e., a successful hopping] occurs. The higher rate of conductivity increase with frequency in region 1 compared with region 2 is probably because here the charge carriers may pass by the side of the nanojacket through the POMA shell. However, at relatively higher frequency (region 2), the charge carriers may enter into the nanojacket in a larger fraction compared with that in region 1 and instead of the increased ratio of successful to unsuccessful hopping a small decrease occurs with an increase in the frequency. In the nanojacketed morphology of dsDNA, the charge carriers may become trapped within the DNA base pairs inside the nanojacket, causing a lower ratio of successful hopping. At the high frequency range (region 3 of Figure 14), the sharp ac-conductivity corresponds to the reorientational (localized) hopping and it increases with an increase in frequency, contributing to a sharp increase of conductivity with frequency.

DISCUSSION

Here we would like to shed light on the probable mechanism of nanojacket formation from the in situ polymerization of POMA in the presence of ds-DNA using $HAuCl_4$ as an oxidant. The spectral data presented above yield the primary results regarding the presence of different components and their interaction in the nanojacketed system. For example, the CD spectrum in organic medium indicates the presence of DNA in the nanojacket where the outer surface is occupied by POMA in the Au–POMA jacket (cf. TEM); FTIR spectra indicate the interaction between POMA and AuNPs and AuNPs and DNA in the jacketed state from the shifting of the benzenoid ring deformation and P–O–C vibration, respectively; XPS spectral data illustrate interaction between the phosphate backbone of DNA and AuNPs; XRD data support the concomitant formation of AuNPs and POMA; and finally impedance analysis of the DNA-nanojacketed system exhibits both resistive and capacitive nature. The spectroscopic characterizations, therefore, assist us to conclude that DNA is present in the DNA–Au–POMA hybrid with retention of its conformation. Considering these points, we propose a probable mechanism of the formation of a nanojacketed DNA morphology as follows.

At first, the monomer molecules (OMA) interact with protonated DNA and become organized around the DNA surface through a weak electrostatic interaction.[16,19] When the $HAuCl_4$ is added to the system, the $AuCl_4^-$ ions immediately interact with the phosphate groups of DNA due to its stronger affinity than OMA, producing an intermediate complex (Scheme 2) and it is probably appropriate particularly for a short time period of reaction.[65] According to Pillai et al., the

dx.doi.org/10.1021/jp412373m | J. Phys. Chem. B XXXX, XXX, XXX–XXX

$AuCl_4^-$ ions interact with the phosphate group at the initial stage and then it can also interact with the base pairs of DNA after a long time interval.[65] In our synthetic procedure, the polymerization starts instantaneously just after the addition of $HAuCl_4$ solution with simultaneous formation of AuNPs. Thus, it is reasonable to think that $AuCl_4^-$ interacts with the phosphate groups of DNA and the so formed negatively charged Au complex electrostatically interacts with the protonated OMA present near the periphery of DNA. Au^{3+} of the complex immediately gets reduced to Au(0), and a concomitant oxidative polymerization of OMA takes place. Due to the large surface area of DNA, this process take place very rapidly (cf. surface catalysis), causing the Au(0) to grow very fast, and with the passage of time, the newly grown AuNPs become very closely spaced on the DNA surface, producing a jacket on DNA which remains at the interior layer of the nanojacket. The generated inner surface of the Au nanojacket thus becomes stabilized by DNA (cf. FTIR and XPS spectra), and the outer surface of the Au nanojacket is stabilized by the in situ synthesized POMA (FTIR spectra), which makes the hybrid soluble in organic medium. As a result, DNA can move from aqueous medium to organic medium using a AuNP–POMA coating.

After treatment with saturated iodine solution, the AuNPs become oxidized to Au^{3+} which are removed from the experimental solution using dialysis. The iodine solution probably diffuses through the channel of the nanojacket by capillary action and interacts from the inner side of the nanojacket due to the oxidative property of iodine. As a result, the nanojacket structure of Au is disrupted, producing the Au^{3+} and leaving the tubular structure of POMA. The free ds-DNA then comes to the aqueous medium which is characterized from the CD spectrum (Figure 7, inset), and the remnant polymer hollow tube is characterized by TEM.

CONCLUSION

In conclusion, a simple procedure of nanojacketing DNA is evolved by synthesizing POMA at room temperature using $HAuCl_4$ as an oxidant and DNA as a soft template. The TEM pictures indicate that AuNPs coat DNA in the form of a nanojacket and the in situ synthesized polymer creates the outer shell adhering to the Au nanojacket. This leads to the easy transfer of DNA from aqueous layer to organic layer without changing the secondary structure of DNA, as evident from CD spectroscopy. Stepping forward to dejacket DNA, the DNA–Au–POMA system was digested with saturated iodine solution for 5 h where DNA comes out with retention of conformation, leaving the POMA nanotube. These procedures may be used to produce a protective coating on DNA, which makes DNA intact in organic medium and may be dejacketed in a facile way with an intact conformation. This procedure can be used to preserve DNA at room temperature for a long time. Further, the DNA–Au–POMA sample exhibits impedometric behavior, and from the Nyquist plot, the values of capacitance and electron-transfer resistance of the material (R_{et}) are calculated to be 13.74 pF and 388 kΩ, respectively. The presence of a single Debye peak in both the impedance and modulus vs frequency plots suggests an isotropic nature of the system. The frequency dependent ac-conductivity plot suggests the presence of short-range translational and reorientational (localized) hopping at lower and higher frequency regions, respectively.

AUTHOR INFORMATION

Corresponding Author

*E-mail: psuakn@iacs.res.in.

Notes

The authors declare no competing financial interest.

ACKNOWLEDGMENTS

S.N. and A.K. acknowledge CSIR, New Delhi, for providing the fellowship. We also acknowledge Mr. Tanmoy Paul of Department of Solid State Physics, IACS, for his help in fitting the impedance curve. Also, we acknowledge "DST Unit of Nanoscience at IACS" for extending TEM and XPS facilities.

REFERENCES

(1) Lassalle, N.; Mailley, P.; Vieil, E.; Livache, T.; Roget, A.; Correia, J. P.; Abrantes, L. M. Electronically Conductive Polymer Grafted with Oligonucleotides as Electrosensors of DNA Preliminary Study of Real Time Monitoring by in Situ Techniques. *J. Electroanal. Chem.* **2001**, *509*, 48–57.

(2) Braun, E.; Eichen, Y.; Sivan, U.; Yoseph, G. B. DNA-Templated Assembly and Electrode Attachment of a Conducting Silver Wire. *Nature* **1998**, *391*, 775–778.

(3) Niemeyer, C. M. Nanoparticles, Proteins, and Nucleic Acids: Biotechnology Meets Materials Science. *Angew. Chem., Int. Ed.* **2001**, *40*, 4128–4158.

(4) Monson, C. F.; Woolley, A. T. DNA-Templated Construction of Copper Nanowires. *Nano Lett.* **2003**, *3*, 359–363.

(5) Mertig, M.; Ciacchi, L. C.; Seidel, R.; Pompe, W. DNA as a Selective Metallization Template. *Nano Lett.* **2002**, *2*, 841–844.

(6) Petty, J. T.; Zheng, J.; Hud, N. V.; Dickson, R. M. DNA-Templated Ag Nanocluster Formation. *J. Am. Chem. Soc.* **2004**, *126*, 5207–5212.

(7) Seidel, R.; Ciacchi, L. C.; Weigel, M.; Pompe, W.; Mertig, M. Synthesis of Platinum Cluster Chains on DNA Templates: Conditions for a Template-Controlled Cluster Growth. *J. Phys. Chem. B* **2004**, *108*, 10801–10811.

(8) Braun, E.; Keren, K. From DNA to Transistors. *Adv. Phys.* **2004**, *53*, 441–496.

(9) Grosber, A. Y.; Nguyen, T. T.; Shklovskii, B. I. *Colloquium*: The Physics of Charge Inversion in Chemical and Biological Systems. *Rev. Mod. Phys.* **2002**, *74*, 329–345.

(10) Gelbart, W. M.; Bruinsma, R. F.; Pincus, P. A.; Parsegian, V. A. DNA-Inspired Electrostatics. *Phys. Today* **2000**, *53*, 38–44.

(11) Endres, R. G.; Cox, D. L.; Singh, R. R. P. *Colloquium*: The Quest for High-Conductance DNA. *Rev. Mod. Phys.* **2004**, *76*, 195–214.

(12) Jaiswal, J. K.; Mattoussi, H.; Mauro, J. M.; Simon, S. M. Long-Term Multiple Color Imaging of Live Cells Using Quantum Dot Bioconjugates. *Nat. Biotechnol.* **2003**, *21*, 47–51.

(13) Chan, W. C. W.; Maxwell, D. J.; Gao, X. H.; Balley, R. E.; Han, M. Y.; Nie, S. M. Luminescent Quantum Dots for Multiplexed Biological Detection and Imaging. *Curr. Opin. Biotechnol.* **2002**, *13*, 40–46.

(14) Sweeney, R. Y.; Mao, C.; Geo, X.; Burt, J. L.; Belcher, A. M.; Georgiou, G.; Iverson, B. L. Bacterial Biosynthesis of Cadmium Sulfide Nanocrystals. *Chem. Biol.* **2004**, *11*, 1553–1559.

(15) Eichen, Y.; Braun, E.; Sivan, U.; Ben-Yoseph, G. Self-Assembly of Nanoelectronic Components and Circuits Using Biological Templates. *Acta Polym.* **1998**, *49*, 663–670.

(16) Nagarajan, R.; Liu, W.; Kumar, J.; Tripathy, S. K.; Bruno, F. F.; Samuelson, L. A. Manipulating DNA Conformation Using Intertwined Conducting Polymer Chains. *Macromolecules* **2001**, *34*, 3921–3927.

(17) Uemura, S.; Shimakawa, T.; Kusabuka, K.; Nakahira, T.; Kobayashi, N. Template Photopolymerization of Dimeric Aniline by Photocatalytic Reaction with $Ru(bpy)_3^{2+}$ in The Presence of DNA. *J. Mater. Chem.* **2001**, *11*, 267–268.

(18) Kobayashi, N.; Uemura, S.; Kusabuka, K.; Nakahira, T.; Takahashi, H. An Organic Red-Emitting Diode with a Water-Soluble

DNA−Polyaniline Complex Containing $Ru(bpy)_3^{2+}$. *J. Mater. Chem.* **2001**, *11*, 1766−1768.
(19) Ma, Y.; Zhang, J.; Zhang, G.; He, H. Polyaniline Nanowires on Si Surfaces Fabricated with DNA Templates. *J. Am. Chem. Soc.* **2004**, *126*, 7097−7101.
(20) Gaylord, B. S.; Heeger, A. J.; Bazan, G. C. DNA Hybridization Detection with Water-Soluble Conjugated Polymers and Chromophore-Labeled Single-Stranded DNA. *J. Am. Chem. Soc.* **2003**, *125*, 896−900.
(21) Thompson, L. A.; Kowalik, J.; Josowicz, M.; Janata, J. Label-Free DNA Hybridization Probe Based on a Conducting Polymer. *J. Am. Chem. Soc.* **2003**, *125*, 324−325.
(22) Wang, J.; Jiang, M. Toward Genolelectronics: Nucleic Acid Doped Conducting Polymers. *Langmuir* **2000**, *16*, 2269−2274.
(23) Wallace, G. G.; Kane-Maguire, L. A. P. Manipulating and Monitoring Biomolecular Interactions with Conducting Electroactive Polymers. *Adv. Mater.* **2002**, *14*, 953−960.
(24) Wilson, E. K. DNA's Conductance Still Confounds. *Chem. Eng. News* **1998**, *76*, 51−54.
(25) Liu, B.; Bazan, G. C. Interpolyelectrolyte Complexes of Conjugated Copolymers and DNA: Platforms for Multicolor Biosensors. *J. Am. Chem. Soc.* **2004**, *126*, 1942−1943.
(26) Sergeyev, V. G.; Pyshkina, O. A.; Lezov, A. V.; Mel'nikov, A. B.; Ryumtsev, E. I.; Zezin, A. B.; Kabanov, V. A. DNA Complexed with Oppositely Charged Amphiphile in Low-Polar Organic Solvents. *Langmuir* **1999**, *15*, 4434−4440.
(27) Ijiro, K.; Okahata, Y. A DNA-Lipid Complex Soluble in Organic Solvents. *J. Chem. Soc., Chem. Commun.* **1992**, 1339−1341.
(28) Ganguli, M.; Jayachandran, K. N.; Maiti, S. Nanoparticles from Cationic Copolymer and DNA That Are Soluble and Stable in Common Organic Solvents. *J. Am. Chem. Soc.* **2004**, *126*, 26−27.
(29) Chiang, J. C.; MacDiarmid, A. G. 'Polyaniline': Protonic Acid Doping of the Emeraldine Form to the Metallic Regime. *Synth. Met.* **1986**, *13*, 193−205.
(30) Li, X. G.; Huang, M. R.; Feng, W.; Zhu, M. F.; Chen, Y. M. Facile Synthesis of Highly Soluble Copolymers and Sub-Micrometer Particles from Ethylaniline with Anisidine and Sulfoanisidine. *Polymer* **2004**, *45*, 101−115.
(31) Kilmartin, P. A.; Trier, L.; Wright, G. A. Corrosion Inhibition of Polyaniline and Poly(o- methoxyaniline) on Stainless Steels. *Synth. Met.* **2002**, *131*, 99−109.
(32) Mattoso, L. H. C.; Faria, R. M.; Bulhoes, L. O. S.; MacDiarmid, A. G. Synthesis, Doping, and Processing of High Molecular Weight Poly (o-methoxyaniline). *J. Polym. Sci., Part A: Polym. Chem.* **1994**, *32*, 2147−2153.
(33) Gazotti, W. A., Jr.; De Paoli, M.-A. High Yield Preparation of a Soluble Polyaniline Derivative. *Synth. Met.* **1996**, *80*, 263−269.
(34) Jamal, R.; Abdiryim, T.; Ding, Y.; Nurulla, I. Comparative Studies of Solid-State Synthesized Poly(*o*-methoxyaniline) Doped with Organic Sulfonic Acids. *J. Polym. Res.* **2008**, *15*, 75−82.
(35) Tan, Y.; Bai, F.; Wang, D.; Peng, Q.; Wang, X.; Li, Y. Template-Free Synthesis and Characterization of Single-Phase Voided Poly(*o*-anisidine) and Polyaniline Colloidal Spheres. *Chem. Mater.* **2007**, *19*, 5773−5778.
(36) Dawn, A.; Nandi, A. K. Nanostructured Self-Assembly of Double-Stranded DNA/Poly(*o*-methoxyaniline) Hybrid. *J. Phys. Chem. C* **2007**, *111*, 6268−6274.
(37) Huang, K.; Zhang, Y.; Long, Y.; Yuan, J.; Han, D.; Wang, Z.; Niu, L.; Chen, Z. Preparation of Highly Conductive, Self-Assembled Gold/Polyaniline Nanocables and Polyaniline Nanotubes. *Chem.—Eur. J.* **2006**, *12*, 5314−5319.
(38) Macdonald, J. R. *Impedance Spectroscopy*; Wiley: New York, 1987.
(39) Gabrielli, C. *Use and Application of Electrochemical Impedance Techniques*; Solartron Analytical: Farnborough, U.K., 1990.
(40) Dias, F. B.; Plomp, L.; Veldhuis, J. B. J. Trends in Polymer Electrolytes for Secondary Lithium Batteries. *J. Power Sources* **2000**, *88*, 169−191.
(41) Wang, X.; Xiao, P. Nondestructive Characterisation of Alumina/Silicon Carbide Nanocomposites Using Impedance Spectroscopy. *J. Eur. Ceram. Soc.* **2000**, *20*, 2591−2599.
(42) Sinclair, D. C.; West, A. R. Impedance and Modulus Spectroscopy of Semiconducting BaTiO3 Showing Positive Temperature Coefficient of Resistance. *J. Appl. Phys.* **1989**, *66*, 3850−3856.
(43) Karmakar, A.; Ghosh, A. Ac Conductivity and Relaxation in CdO Doped Poly Ethylene Oxide-LiI Nanocomposite Electrolyte. *J. Appl. Phys.* **2011**, *110*, 034101-1−034101-6.
(44) Paul, T.; Ghosh, A. Conduction and Relaxation Mechanisms in Bismuth Doped $La_2Mo_2O_9$ Ionic Conductors. *J. Appl. Phys.* **2013**, *114*, 164101-1−164101-7.
(45) Dawn, A.; Nandi, A. K. Biomolecular Hybrid of a Conducting Polymer with DNA: Morphology, Structure, and Doping Behavior. *Macromol. Biosci.* **2005**, *5*, 441−450.
(46) Dawn, A.; Nandi, A. K. Slow Doping Rate in DNA-Poly(*o*-methoxyaniline) Hybrid: Uncoiling of Poly(*o*-methoxyaniline) Chain on DNA Template. *Macromolecules* **2005**, *38*, 10067−10073.
(47) Wang, X.; Ray, S.; Cooney, R. P.; Kilmartin, P. A.; Waterhouse, G. I. N.; Easteal, A. J. Synthesis and Characterization of Poly(o-methoxyaniline)−Lignosulfonate Composites. *Synth. Met.* **2012**, *162*, 1084−1089.
(48) Ruokolainen, J.; Eerika1inen, H.; Torkkeli, M.; Serimaa, R.; Jussila, M.; Ikkala, O. Comb-Shaped Supramolecules of Emeraldine Base Form of Polyaniline Due to Coordination with Zinc Dodecyl Benzenesulfonate and Their Plasticized Self-Organized Structures. *Macromolecules* **2000**, *33*, 9272−9276.
(49) Storhoff, J. J.; Lazarides, A. A.; Mucic, R. C.; Mirkin, C. A.; Letsinger, R. L.; Schatz, G. C. What Controls the Optical Properties of DNA-Linked Gold Nanoparticle Assemblies? *J. Am. Chem. Soc.* **2000**, *122*, 4640−4650.
(50) Mukherjee, P.; Nandi, A. K. Growth of Different Shape Au Nanoparticles through an Interfacial Redox Process Using a Conducting Polymer. *Langmuir* **2010**, *26*, 2785−2790.
(51) Sprecher, C. A.; Basse, W. A.; Johnson, W. C. Conformation and Circular Dichroism of DNA. *Biopolymers* **1979**, *18*, 1009−1019.
(52) Dawn, A.; Nandi, A. K. Simple Method for the Preparation of DNA-Poly(*o*-methoxyaniline) Hybrid: Structure, Morphology, and Uncoiling of Poly(*o*-methoxyaniline) on the DNA Surface. *Langmuir* **2006**, *22*, 3273−3279.
(53) Dawn, A.; Mukherjee, P.; Nandi, A. K. Preparation of Size-Controlled, Highly Populated, Stable, and Nearly Monodispersed Ag Nanoparticles in an Organic Medium from a Simple Interfacial Redox Process Using a Conducting Polymer. *Langmuir* **2007**, *23*, 5231−5237.
(54) Garai, A.; Kuila, B. K.; Nandi, A. K. Montmorillonite Clay Nanocomposites of Sulfonic Acid Doped Thermoreversible Polyaniline Gel: Physical and Mechanical Properties. *Macromolecules* **2006**, *39*, 5410−5418.
(55) Mukherjee, P.; Nandi, A. K. Concomitant Synthesis of Polyaniline and Highly Branched Gold Nanoparticles in The Presence of DNA. *J. Colloid Interface Sci.* **2011**, *356*, 145−150.
(56) Rath, S.; Sarangi, S. N.; Sahu, S. N. XPS Studies of DNA−Cation-Interacted Self-Assembled HgTe Quantum Dots Formed Under Electrodeposition and Their Resultant Biomolecular Recognition Application. *Nanotechnology* **2008**, *19*, 115606 1−7.
(57) Sreedhar, B.; Sairam, M.; Chattopadhyay, D. K.; Mitra, P. P.; Mohan Rao, D. V. Thermal and XPS Studies on Polyaniline Salts Prepared by Inverted Emulsion Polymerization. *J. Appl. Polym. Sci.* **2006**, *101*, 499−508.
(58) Wagner, C. D.; Riggs, W. M.; Davis, L. E.; Moulder, J. F.; Muilenberg, G. E. *Handbook of X-ray Photoelectron Spectroscopy*; Perkin-Elmer Corporation: Eden Prairie, MN, 1978.
(59) Kundu, A.; Layek, R. K.; Kuila, A.; Nandi, A. K. Highly Fluorescent Graphene Oxide-Poly(vinyl alcohol) Hybrid: An Effective Material for Specific Au^{3+} Ion Sensors. *ACS Appl. Mater. Interfaces* **2012**, *4*, 5576−5582.
(60) Mukherjee, P.; Nandi, S.; Nandi, A. K. Optoelectronic Properties of RNA−Polyaniline−Dendritic Gold Nanobiocomposite. *Synth. Met.* **2012**, *162*, 904−911.

(61) Mukherjee, P.; Kundu, A.; Samanta, S.; Roy, S.; Nandi, A. K. Nondestructive Characterization of Li^+ Ion-Doped Multifunctional Poly(vinylidene fluoride)-g-poly(dimethyl amino ethyl methacrylate) by Impedance Spectroscopy. *J. Phys. Chem. B* **2013**, *117*, 1458−1466.
(62) Peng, H.; Soeller, C.; Travas-Sejdic, J. Novel Conducting Polymers for DNA Sensing. *Macromolecules* **2007**, *40*, 909−914.
(63) Wang, J. Electrical Conductivity of Double Stranded DNA Measured with Ac Impedance Spectroscopy. *Phys. Rev. B* **2008**, *78*, 245304 1−9.
(64) Barranco, A. P.; Amador, M. P. G.; Huanosta, A.; Valenzuela, R. Phase Transitions in Ferrimagnetic and Ferroelectric Ceramics by Ac Measurements. *Appl. Phys. Lett.* **1998**, *73*, 2039−2041.
(65) Pillai, C. K. S.; Nandi, U. S. Interaction of Metal Ions with Nucleic Acids and Related Compounds. II. Studies on Au(III)-Nucleic Acid System. *Biopolymers* **1978**, *17*, 709−729.